ACS APPLIED MATERIALS & INTERFACES

Research Article

www.acsami.org

A Shape-Recovery Polymer Coating for the Corrosion Protection of Metallic Surfaces

Alexander Lutz,*[,†,‡,∥] Otto van den Berg,*[,‡,§,∥] Jonas Van Damme,[§] Karen Verheyen,[⊥] Erwin Bauters,[⊥] Iris De Graeve,[†] Filip E. Du Prez,[§] and Herman Terryn[†]

[†]Department of Materials and Chemistry, Research Group Electrochemical and Surface Engineering, Vrije Universiteit Brussel, Pleinlaan 2, 1050 Brussels, Belgium

[‡]SIM vzw, Technologiepark 935, 9052 Zwijnaarde, Belgium

[§]Department of Organic and Macromolecular Chemistry, Polymer Chemistry Research Group, Ghent University, Krijgslaan 281, S4-bis, B-9000 Ghent, Belgium

[⊥]Flamac, Technologiepark 903, 9052 Zwijnaarde, Belgium

Supporting Information

ABSTRACT: Self-healing polymer coatings are a type of smart material aimed for advanced corrosion protection of metals. This paper presents the synthesis and characterization of two new UV-cure self-healing coatings based on acrylated polycaprolactone polyurethanes. On a macroscopic scale, the cured films all show outstanding mechanical properties, combining relatively high Young's modulus of up to 270 MPa with a strain at break above 350%. After thermal activation the strained films recover up to 97% of their original length. Optical and electron microscopy reveals the self-healing properties of these coatings on hot dip galvanized steel with scratches and microindentations. The temperature-induced closing of such defects restores the corrosion protection and barrier properties of the coating as shown by electrochemical impedance spectroscopy and scanning vibrating electrode technique. Therefore, such coatings are a complementary option for encapsulation-based autonomous corrosion protection systems.

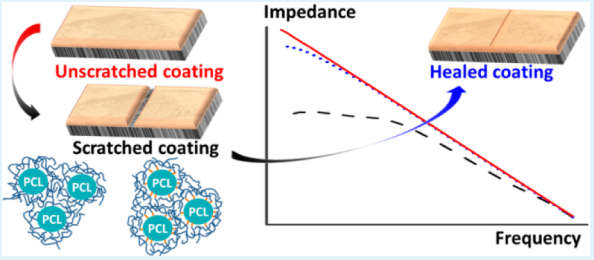

KEYWORDS: *self-healing coatings, polycaprolactone, smart materials, SVET, corrosion protection*

INTRODUCTION

The worldwide most-used metals like iron and aluminum have the disadvantage of thermodynamic instability of their metallic form. Consequently, a wide range of corrosion protection mechanisms exist to extend product lifetime in various conditions: passivation, alloying, cathodic protection, sacrificial metallic coatings like hot dip galvanized (HDG) steel,[1] barrier coatings, and a plethora of corrosion inhibitors.[2−4] The application of organic coatings and paints not only gives a color to the metal and provides better processability but also hinders corrosive species from reaching the metal surface. In this way, organic coatings can provide outstanding corrosion protection. However, when a small defect is made in the coating, and the metal surface is exposed to an aggressive solution, it will immediately start to corrode with disastrous effects on the adhesion of the coating and the integrity of the coated object. Such defects can not only occur when a product is used but also already during its production, for example, during forming processes of precoated metal sheets. The addition of corrosion inhibitors to the coating system is an established approach to improve the corrosion protection. Some corrosion inhibitors specifically act on sites of corrosive attack and locally inhibit corrosion, which is why such coatings were the first to be called "self-healing".[5−7]

In the last two decades this term has been used for a range of developments for local, autonomous, and on-demand corrosion inhibitor release from different inhibitor containers.[8−14] For example, Maia et al. produced silica nanocapsules with increased inhibitor release at elevated pH,[12] whereas the groups of Zheludkevich, Buchheit, and McMurray proposed clays and organic ion-exchange materials, which release the inhibitor in exchange for aggressive chloride ions.[9,15,16] Very recently, synergistic corrosion protection effects were achieved by various combinations of different nanocontainers in epoxy coatings.[13,17] However, coatings based on this self-healing principle inhibit corrosion but do not close the defect, nor do they re-establish the barrier properties of the polymeric coating.

Filling of scratches and defects is a completely different protection mechanism and is independent of the self-healing mechanism described above. The White and Sottos group were the first who encapsulated a healing agent to fill defects in

Received: August 21, 2014
Accepted: December 17, 2014
Published: December 17, 2014

DOI: 10.1021/am505621x
ACS Appl. Mater. Interfaces 2015, 7, 175−183

polymers.[18] Upon breakage of the microcapsules, dicyclopentadiene was released and initiated the healing in an epoxy matrix. Similarly, Caruso et al. achieved 82% fracture toughness recovery of a polymer with encapsulated solvents.[19] Although fully autonomous, such extrinsic healing mechanisms are limited to the amount and the size of capsules in the coating and relatively small defects.[20] A microvascular system (two- or three-dimensional) incorporated in the coating allows much larger defects to be healed, though technological implementation is difficult.[21−23] However, these systems demonstrate repeatable healing. The class of self-healing polymers based on intrinsic healing effects shows also repeatable healing ability.[24] Their healing functionality is theoretically undepletable, but they need some kind of trigger. Additionally, intrinsically self-healing polymers have less defect size limitations than capsule-based systems.[25−27] The most prominent mechanism is based on the Diels−Alder reaction, which is reversible at ∼120 °C.[27−30] However, any mechanism where a chemical reaction takes place has the possibility of undesired irreversible side reactions, which permanently reduce the healing efficiency. Therefore, our choice was a physicochemical mechanism, that is, the shape memory or shape recovery effect. The stress or strain induced in a shape-recovery material by mechanical deformation can be fully reversed by heating without any chemical reaction taking place.[30−32] In detail this effect is possible because of a multiple phase structure with different glass transition (T_g) or melting temperatures (T_m). One phase of the segmented block copolymer network melts, whereas the other keeps its solid form. This property gives the polymer on the one hand enough mobility for strain recovery and on the other hand enough stability to keep its shape. Rodriguez et al. blended linear polycaprolactone (PCL) with a cross-linked PCL network.[33] The shape-recovery properties of the cross-linked PCL network assist with the scratch closure before self-healing by interdiffusion of the linear PCL chains over the crack surface takes place (shape memory assisted self-healing or "SMASH"). This principle has been very recently combined with Diels−Alder chemistry (DASMASH) to additionally covalently reform the reversible cross-links of thermoremendable shape memory polyurethanes (PUs).[34] D'Hollander et al. have shown that several segmented PCL-based $(AB)_n$ polymers show excellent shape memory-based characteristics.[35] Applied as a coating on a metallic substrate, it has the ability to close scratches as demonstrated by Gonzales-Garcia et al. with optical and electrochemical microscopy and Jorcin et al. using "odd random phase electrochemical impedance spectroscopy" (ORP-EIS).[26,36] However, the production of a coating, using a technique that requires the use of a toxic and/or high-boiling organic solvent, is not feasible for large-scale coating application.

UV-cure coatings have received much attention in recent times and often are 100% solvent-free. Except for the photoinitiator, all molecules in the liquid resin react during curing, and no solvents (organic or aqueous) need to be evaporated. The wet thickness of such a coating before curing is thus the same as the dry thickness after curing, because no solvent needs to evaporate. In addition, the use of energy during application and curing is low, because of efficient polymerization initiation and no need of thermal energy for solvent evaporation. The most common way to formulate a 100% radiation cure-type coating is to combine a multifunctional acrylated oligomer (two or more acrylate moieties per chain) with a low molecular weight acrylate (mono or multifunctional) that acts as a reactive solvent for the oligomeric acrylate resin. After addition of a photoinitiator, application on a substrate, and exposure to UV radiation, a film is formed within a fraction of a second. Polycaprolactone is a well-known material for preparation of reactive oligomers, including urethane-based acrylates.[37,38] However, the use of higher molecular weight polycaprolactone acrylates as coating resins is an unexplored area of research, probably because of viscosity issues and a lack of (formulation) stability caused by crystallization of high molecular weight PCL from solution at ambient temperature. With specific modifications of both the polycaprolactone resin and the formulation composition, we aim to circumvent these issues by making use of the excellent shape-recovery properties of high molecular weight polycaprolactone.

Within this publication, we focus on the shape-recovery and corrosion-protection properties of the coating. We present the thermal properties of the coating and its components based on differential scanning calorimetry (DSC) measurements and show its mechanical strength and flexibility with tensile tests aiming for future industrial application. On the basis of thermal relaxation experiments, we discuss the shape-recovery properties of the polymer network and show that the different segments in the polymer network have different effects on the healing. In the second part, we evaluate the healing of the polymer applied as a coating on HDG steel with optical and electron microscopy. Conventional and local electrochemical techniques show the recovery of the coating's barrier properties and corrosion-protection properties. As a comparison, the authors discuss the influence of the introduction of flexible spacers into the polymer structure and demonstrate the coatings' properties as a novel corrosion-protection system.

The on-demand self-healing functionality of the coating allows the owner of a product to increase the product lifetime by closing defects, thereby stopping the corrosion attack and thus saving corrosion inhibitor reservoirs.

EXPERIMENTAL SECTION

Materials. 1,6-Diisocyanatohexane (HDI, >99%), dibutyltin dilaurate (DBTL), hydroxyethyl acrylate (HEA, 96%), high-performance liquid chromatography grade toluene (dried over sodium and distilled prior to use), and isobornyl acrylate (IBOA, >85%) were purchased from Sigma-Aldrich Co. HEA was dried over 4 Å molecular sieves prior to use. Pripol 2033 fatty dimer diol was obtained from Croda Chemicals. Hydroxyl-functional telechelic polycaprolactone (M_n = 6000 g/mol) was obtained from Solvay. HDG Steel (HDG Z350, with a 25 μm thick zinc layer on each side) panels produced by ArcelorMittal were cleaned with Ridoline C72 from Henkel prior to coating application. KIP 160 and 2,2-dimethoxy-2-phenylacetophenone (DMPA, 99%) were used as photoinitiators for UV curing from Allnex Belgium NV and Sigma-Aldrich, respectively.

Prepolymer Synthesis. Synthesis of telechelic acrylated polycaprolactone (PP_{NF}) hydroxyl-functional telechelic polycaprolactone (100 g, 16.6 mmol) was dried by coevaporation with dry toluene (2 × 100 mL), taking care that all polymer material had dissolved before the toluene was removed. This required heating to approximately 50 °C in a water bath. Dry toluene (300 mL) was added, and the solution was brought under an argon atmosphere. The temperature of the solution was raised to 90 °C in an oil bath, and all 1,6-diisocyanatohexane (5.61 g, 33.3 mmol) was added at once under vigorous stirring. Then three drops of dibutyltin dilaurate were added, and the stirring was continued for 60 min. Hydroxyethyl acrylate (3.87 g, 33.3 mmol) was added, and the stirring was continued for another 60 min at 90 °C. Finally the solution was precipitated in cold methanol. The prepolymer was then dried under vacuum yielding PP_{NF} (105 g, 96%) as a white fluffy solid. ^{1}H NMR (300 MHz, $CDCl_3$): 6.37 (dd, 0.017H, $\underline{H}CH{=}CH-$), 6.07 (dd, 0.017H, $HC\underline{H}{=}CH-$), 5.79 (dd, 0.017H, $HCH{=}C\underline{H}-$), 4.75 (s, 0.013H, $O-CH_2-CH_2-O\text{-}C{=}ON\underline{H}-$), 4.67 (s, 0.027H, $CH_2-CH_2-CH_2-O-C{=}ON\underline{H}-$), 4.25 (m, 0.075H, $-O-C\underline{H_2}C\underline{H_2}O-$), 3.99 (t,

DOI: 10.1021/am505621x
ACS Appl. Mater. Interfaces 2015, 7, 175−183

2H, C$\underline{H_2}$O−), 3.09 (m, 0.12H, C$\underline{H_2}$NHC=O), 2.24 (t, 2H, C$\underline{H_2}$C=O), 1.58 (m, 4H, O=C−CH_2C$\underline{H_2}$$CH_2C\underline{H_2}$$CH_2$O−), 1.33 (m, 2H, O=C−$CH_2CH_2C\underline{H_2}$$CH_2$ CH_2O−).

Synthesis of Telechelic Acrylated Polycaprolactone with Flexible Spacers. A mixture of hydroxyl-functional telechelic polycaprolactone (100 g, 16.6 mmol) and Pripol 2033 fatty dimer diol (17.9 g, 33.3 mmol) as flexible spacers was dried by coevaporation with dry toluene (2 × 100 mL), taking care that all polymer material had dissolved before the toluene was removed. This required heating to approximately 50 °C in a water bath. Dry toluene (300 mL) was added, and the solution was brought under an argon atmosphere. The temperature of the solution was raised to 90 °C in an oil bath, and 1,6-diisocyanatohexane (11.2 g, 66.7 mmol) was added all at once under vigorous stirring like in the synthesis of PP_{NF}. Three drops of dibutyltin dilaurate were added, and the stirring was continued for 60 min. Hydroxyethyl acrylate (3.87g, 33.3 mmol) was added, and the stirring was continued for another 60 min at 90 °C. Finally the solution was precipitated in cold methanol. The prepolymer was then dried under vacuum yielding telechelic acrylated polycaprolactone with flexible spacers (PP_{FL}, 121 g, 94%) as a white fluffy solid. ^{1}H NMR (300 MHz, $CDCl_3$): 6.44 (dd, 0.019H, $\underline{H}$CH=CH−), 6.15 (dd, 0.019H, HC$\underline{H}$=CH−), 5.86 (dd, 0.019H, HCH=C$\underline{H}$−), 4.82 (s, 0.018H, O−CH_2−CH_2−O−C=ON$\underline{H}$−), 4.72 (s, 0.096H, CH_2−CH_2−CH_2−O-C=ON$\underline{H}$−), 4.32 (m, 0.097H, −O−C$\underline{H_2}$C$\underline{H_2}$O−), 4.06 (t, 2.2H, C$\underline{H_2}$O−), 3.15 (m, 0.25H, C$\underline{H_2}$NHC=O), 2.31 (t, 2H, C$\underline{H_2}$C=O), 1.0−1.8 (m, 8.72H, CH_2 alkyl), 0.87 (m, 0.27H, CH_3).

Coating Formulation and Application. The coating resins (R_{NF} and R_{FL}) were formulated as 60/40 IBOA/PP_{NF} and 50/50 IBOA/PP_{FL} mixtures, respectively. The ratios were chosen to have equal amounts of PCL (36 mol %) in them, without having formulation viscosities that are either too low or too high for suitable application (1000 cPs < X <15 000 cPs). 2,2-Dimethoxy-2-phenylacetophenone (10 mg/g) was added for curing of 1−2 mm thick samples for polymer tests, using a low-intensity mercury vapor lamp.

For the coatings on HDG steel, 10 mg/g of KIP 160 was added to the above-described resins that were heated to 60 °C before application. The HDG steel panels were first cleaned by acetone rinsing, then immersed for 3−5 s in a 10% solution of Ridoline C72 at 60 °C and then rinsed twice with distilled water. After drying the panels by pressurized air, they were coated with a "doctor blade" (100 μm wet coating thickness). Subsequently, the panels were UV-cured by irradiation under two UV lamps (D- and H-lamp) with a total power of 236 W/cm under a nitrogen atmosphere and at a speed of 30 cm/s. Samples prepared with R_{NF}, containing PP_{NF}, without flexible spacers are referred to with the abbreviation NF, whereas samples prepared with R_{FL}, containing PP_{FL}, including flexible spacers, are referred to as FL.

Thermomechanical Polymer Characterization. DSC was performed on a DSC Q2000 from TA Instruments with samples of ∼7 mg in hermetically sealed pans. Tensile testing was performed on a Tinus-Olsen H10KT tensile tester equipped with a 100 N load cell, using flat standard dog bone-type specimen with an effective gage length of 13 mm, a width of 2 mm, and a thickness of 1 mm. The tensile tests were run at a speed of 1 mm/min. Test specimens were prepared by injection of the formulation between glass plates fitted with 1 mm silicone spacers, leaving open spaces all around the liquid formulation to allow shrinkage in the lateral direction. Photocuring was performed at an approximate light intensity (365 nm) of 12 mW/cm^2 in a Metalight Classic irradiation chamber for 5 min. After cooling, samples were cut from the sheets using a Ray-Ran dog bone cutter. The thermal recovery was measured on a Q800 series DMTA in tensile mode at a heating rate of 2.5 °C/min up to a temperature of 130 °C.

Microscopy. The microscopy images were taken with a top view digital camera (UI-1640LE-C-HQ) from IDS Imaging Development Systems GmbH (Germany) with a 1 MPixel resolution, which was part of the scanning vibrating electrode technique (SVET) system. To record the healing stages of the coating, a heating plate was installed under the microscope objective, and pictures were taken regularly with the ASET LV2 software from Science Wares, Inc. during the heating process. Secondary electron (SE) images were taken with a Phenom Pro X (Phenom-World BV, The Netherlands) at 5 kV in charge reduction mode. A standard scalpel knife was used to make the scratches in the microscopy samples.

Electrochemical Techniques. For all electrochemical tests, the coated HDG samples were covered with adhesive tape (3 M polyester tape No. 8402) except for the measurement area—a circle of 1.1 cm^2. The samples were immersed in 0.05 M sodium chloride (NaCl) solution and were left for 5−30 min until a stable open circuit potential (OCP) was reached. Electrochemical impedance spectroscopy (EIS) was performed using an Autolab 302N potentiostat from Metrohm AG (Swiss) and a standard three-electrode setup. 49 frequencies were excited, logarithmically equally distributed over the whole measurement range from 10^5 to 10^{-1} Hz with an amplitude of 10 mV rms. SVET measurements were performed using a SVET from Applicable Electronics, LLC, in combination with the ASET software from Science Wares Inc. (USA). Every 35 μm one measurement point of the vertical component of the current density was recorded to build up the entire current density map. A screwdriver was sharpened with sand paper of 500, 1200, and finally 4000 grit to create a knifelike edge. Defects of ∼50 by 500 μm for SVET analysis were made by pushing this handmade microchisel perpendicularly to the surface into the coating. Full penetration of the organic coating, exposing the underlying HDG steel, was confirmed under an optical microscope. For SVET the measurement area not covered by tape was ∼1 × 2 mm.

RESULTS AND DISCUSSION

Coating Resin. For the preparation of a self-healing coating, mobility, whether on molecular, segmental, or macroscopic scale, is required in at least one form to facilitate the healing process.[39] A radical-initiated UV-cure coating has little or no volatile organic compounds content and requires little energy input for curing. Such coatings usually consist of two main structural components that make up the majority of the coating formulation.[40] Generally an oligomeric acrylated resin is combined with a low molecular weight (multi)functional acrylate monomer that acts as a reactive diluent. After irradiation, an intricate network is formed where both the reactive diluent and the resin can act as cross-linkers, resulting in an insoluble, immobile coating material. To introduce mobility into the final coating material, several measures can be taken. First, a monofunctional reactive diluent can be used that leads to the formation of long linear acrylate chains. Second, a high molecular weight acrylated resin with limited functionality can be introduced to keep the overall cross-link density low. These measures will, however, also decrease the solvent resistance and the strength of the coating. To minimize these undesired effects, a reactive diluent was chosen that, after cure, results in a polymer with a low cross-link density, but with a T_g far above room temperature and thereby compensating these undesired effects without introducing too much rigidity. IBOA is a monomer widely used in industrial applications where a high T_g of the final cured product is required.[41] With a T_g of ∼94 °C it was the material of choice.[42] As cross-linker, a relatively high molecular weight commercial PCL diol was used as starting material. A DBTL-catalyzed reaction with 2 equiv of HDI at 90 °C in dry toluene led to the formation of a PCL−urethane prepolymer that was acrylate end-capped by addition of 2 equiv of HEA, yielding PP_{NF}. Addition of more than 2 equiv of HEA resulted in the unexpected formation of nonacrylate functional PCL−urethanes due to transesterification reactions of the HEA−urethane end groups with HEA, forming ethylene glycol bisacrylate and hydroxyethylurethane end groups. However, when stoichiometry was maintained, no signs of transesterification were found, and NMR analysis showed nearly 100% functionalization. The resin prepared in the above fashion did not dissolve in IBOA at room temperature, and application on any substrate required

DOI: 10.1021/am505621x
ACS Appl. Mater. Interfaces 2015, 7, 175−183

some heating to keep the resin in solution (vide infra). Although practically possible, heating is not desirable for any coating system.

To increase the compatibility between IBOA and the PCL resin, the PCL diol was chain-extended using a commercially available fatty dimer diol, which imparts flexibility and solubility in hydrocarbon solvents. Thus, by reacting 4 equiv of HDI with a mixture of 1 equiv of PCL diol and 2 equiv of fatty dimer diol, a fatty dimer-modified PCL–urethane prepolymer was obtained that was finally acrylate end-capped by addition of 2 equiv of hydroxyethyl acrylate (HEA), yielding PP_{FL}. Omitting the flexible spacer gave a resin (R_{NF}) that required heating during application to keep the formulation stable, whereas R_{FL} can be applied without preheated substrates.

Scheme 1. Acrylated Urethane-Resin Synthesis[a]

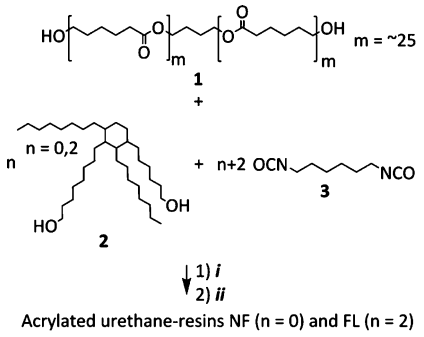

[a]From telechelic hydroxy-functional polycaprolactone (**1**, M_n = 6000 g/mol), fatty dimer diol (**2**, Pripol 2033, a mixture of cyclic and noncyclic structural isomers containing 36 carbon atoms, the structure depicted in this scheme is one of many structures present in Pripol 2033), and hexamethylene diisocyanate (**3**). (i) dibutyltin dilaurate, toluene, 90°C, 1 h. (ii) hydroxyethyl acrylate (2 mol equiv), 90°C, 1 h. Polymers having no Pripol 2033 (n = 0, R_{NF}) and having 2 equiv of Pripol 2033 (n = 2, R_{FL}) were synthesized.

Size exclusion chromatography (SEC) of both R_{NF} (M_n 11 700, M_w 15 000, $Đ$ 1.28) and R_{FL} (M_n 27 000, M_w 42 000, $Đ$ 1.6) shows clear increases in molecular weight compared with the starting PCL diol. (see S.I.1 in the Supporting Information.) Because HDI is a nonselective diisocyanate, a certain degree of polymer–polymer coupling is to be expected depending on statistics only. NMR analysis of R_{NF} shows that the number of end group functionality (acrylate double bonds) is in accordance with the number-average molecular weight (M_n) determined with SEC, indicating full functionalization of the resin. For R_{FL} no such agreement was found, probably because of the formation of short-chain products not taken into account using SEC.

Thermomechanical Characterization. The thermomechanical properties of the two polycaprolactone-containing materials, described in the previous section, were first investigated by DSC, showing the melting peaks of the PCL phases in both kinds of polymer networks. For the polymer with flexible spacers, the melting temperature (T_m) of the PCL phase was derived to be at 49.6 °C, whereas for the one without flexible spacers it was derived to be at 51.7 °C (Figure 1). The steps on the left side of the peaks indicate recrystallization during the melting process with an onset temperature of 33.7 °C and of 39.2 °C, respectively (not shown in Figure 1). Because of the cross-linked nature of the polymer network, the T_g of the IBOA phase could not be determined. The recrystallization of the polymer network with flexible spacers during solidification takes place at

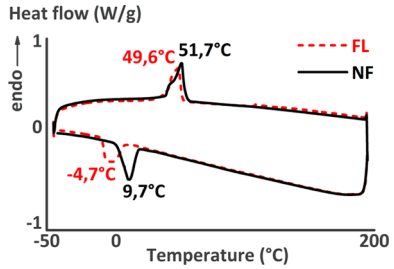

Figure 1. DSC thermograms of the cured coating formulations prepared from R_{NF} containing no flexible spacers (NF) and from R_{FL} containing flexible spacers (FL), showing the melting and crystallization peaks.

15 °C below the one without flexible spacers. The presence of the fully amorphous molecular spacer units in the polymer network delays its recrystallization and shifts the heat-flow peak to lower values. These results are somewhat different compared with those found by D'Hollander et al.,[35] where crystallization of PCL was enhanced, rather than inhibited, by the introduction of flexible units. This difference in behavior can be explained by the presence of hydrogen-bonded crystalline PU segments in the materials prepared by D'Hollander, whereas no such PU segments are present in the materials reported in this paper. Moreover, the idea behind the use of flexible spacers in functional PU resins is to introduce a kind of "surfactant" effect with flexible units in the uncured formulation pointing outward from PCL clusters to inhibit the crystallization from solution. This inhibition of crystallization is preserved in the cured state of the formulation. In the D'Hollander materials the opposite effect is observed; an enhanced crystallization at higher temperatures with little hysteresis.

The mechanical properties of the polymer networks were characterized by tensile tests (Figure 2). The strain at break of

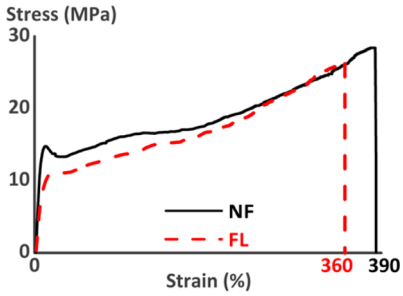

Figure 2. Stress–strain curves of the polymer network with (FL) and without (NF) flexible spacers are very similar.

both polymer networks is similar, 360 and 390% for the FL- and NF-resin, respectively. Their Young's modulus was calculated to be 0.15 and 0.27 GPa, respectively. The introduction of the flexible spacers thus reduces the Young's modulus of the polymer network as expected, but barely changes the stiffness and strain at break. This is not surprising, because the flexible spacers do not alter the main structure of the network.

Strain Recovery. The shape-recovery properties of the polymer were followed by dynamic mechanical analysis (DMA). Both samples were heated to 130 °C, and the strain recovery from initially 150% and 200% strain was recorded. Four effects can be deduced from Figure 3. First, the recovery mechanism changes for both polymer networks at two temperatures. 50% of the strain recovery happens at temperatures below 55 °C. Until ~95 °C, the strain recovery reaches at least 75%, and the rest

DOI: 10.1021/am505621x
ACS Appl. Mater. Interfaces 2015, 7, 175–183

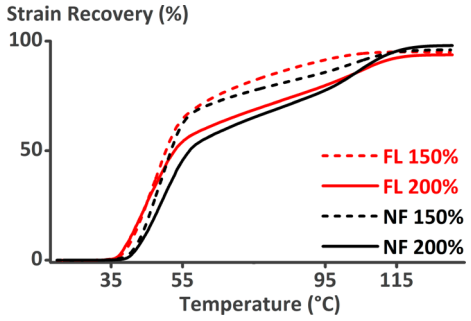

Figure 3. Strain recovery curves of the polymer networks with (FL) and without (NF) flexible spacers, stretched to 150% and 200% recorded with a DMA equipment. All samples show almost full shape recovery when heated above 115 °C.

takes place at higher temperatures. Comparing this fact with the DSC measurements of Figure 1, the main part of the healing is achieved by the recrystallization, which happens just before the melting of the PCL phase (at ∼50 °C). At higher temperatures, the shape recovery continues while the PCL phase is molten (Figure 3). If complete healing has not yet been achieved, such as for the polymer network without flexible spacers and 200% original strain, the surpassing of the T_g of the IBOA phase (The T_g of pure poly(IBOA) is 94 °C.[42]) gives the network enough mobility to fully heal. Because of the different recovery stages (35−55 °C and 55−100 °C), we presume that different phases participate in the healing (melting of the PCL phase, glass transition phenomena of poly(IBOA) phase, respectively); depending on the degree of deformation.

Second, both polymer networks require a lower initial healing temperature for the same amount of partial healing when a lower initial strain was applied. Anyway, as one sees in Figure 3 this effect has no influence on the full strain recovery. The temperature requirements for full healing will be further discussed on coated samples with defects. Third, the polymer with flexible spacers shows higher strain recovery at lower temperatures, which might be ascribed to an earlier (temperature-wise) onset of the PCL phase recrystallization and melting, but slightly lower strain recovery at higher temperatures compared with the NF samples. Fourth, the strain recovery reaches ∼95% at 130 °C for both polymer networks. When thermal expansion is taken into account, this value will be even higher.

In another test, the samples were stretched to 200% strain at room temperature and put in an oven at 90 °C for 5 min. The distance between two marks was compared with the distance before stretching. The procedure was repeated for a second time to prove the repeatability of the shape-recovery properties. Table 1 shows that the shape recovery remains on a similar level. In accordance with Figure 3, the recovery of the NF samples is at this temperature still below the recovery of the FL samples.

Table 1. Summary of the Recovery of the Distance between Two Marks of Dog Bone Samples of the Two Polymer Networks with (FL) and without (NF) Flexible Spacers after Stretching to 200% Strain and Heating to 90°C for 5 min Once and Twice

sample name	recovery after heating [%]	recovery after second cycle [%]
FL	96	97
NF	87	82

Because of the short recovery time at 90 °C compared with the tensile tests in Figure 3, the sample with flexible spacers shows better recovery than the coating without flexible spacers, also after a second deformation. This can be explained by the increased mobility of the coating with flexible spacers. Increasing the recovery time will allow the coating without flexible spacers to have also a higher recovery as shown in Figure 3.

Characterization of the Applied Coating. For this section, the polymer networks were applied as coatings on galvanized steel plates (see Experimental Section), and the corrosion protection properties were tested. Optical and electron microscopy was used for visualization of the defect closure, whereas EIS and SVET showed the recovery of the barrier properties of the healed defects in an aggressive NaCl solution.

The macroscopic self-healing ability of the two coatings was investigated by optical microscopy. The results were similar, and thus only images of the coating without flexible spacers will be presented. Three scratches were made with a scalpel knife into the coating (Figure 4). Because of its transparency, the grain

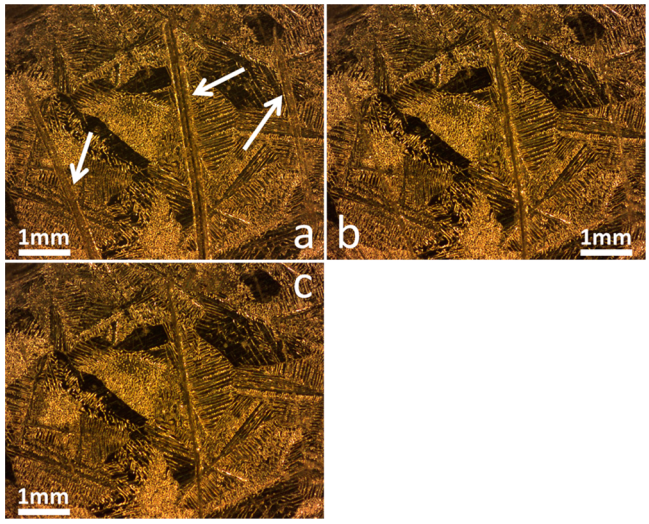

Figure 4. Optical micrographs of three scratches in the transparent self-healing coating on HDG steel (a). The same scratches after heating the sample to 60 °C can be seen in (b) and after heating to 115 °C for a few minutes in (c). White arrows point to the scratches in (a) for better recognizability. The HDG structure underneath the coating is clearly visible.

structure of the underlying zinc layer can clearly be seen. For the two outer scratches, only little force was applied to just superficially scratch the coating. The third scratch in the center was made with higher force to clearly cut through the coating and thus also partially scratch the zinc layer of the HDG steel substrate. The samples were heated on a hot plate mounted underneath a microscope camera. In this way, the closing of the scratches in the self-healing coating could be filmed. The main part of the healing process took place within a few tens of seconds after reaching the melting temperature of the PCL block (Figure 4b), but only after heating to temperatures above the T_g of the hard phase (IBOA), the scars became also invisible (Figure 4c). After 2 min, the scratches were fully closed, and no change of the surface could be detected anymore. Obviously, the scratch in the zinc layer does not heal at these temperatures and thus is still visible underneath the transparent healed coating in Figure 4c. For a better visualization, the authors refer to a short video of the healing in the Supporting Information (S.I.2).

DOI: 10.1021/am505621x
ACS Appl. Mater. Interfaces 2015, 7, 175−183

The coating's defect closing ability on the microscopic scale was verified with secondary electron microscopy. The images in Figure 5 show three scratches of ~50 μm width: The first one is a

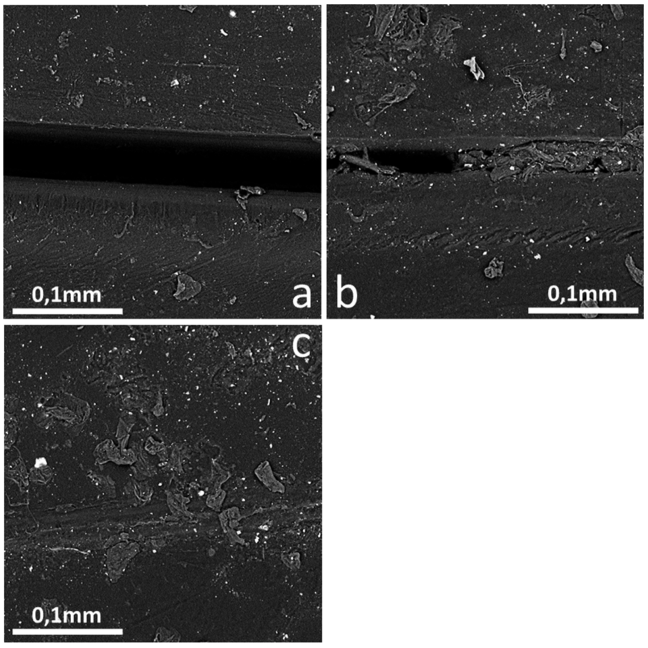

Figure 5. SEM images (1000× magnification) of a scratch (width ca. 50 μm) in the self-healing coating NF (a), a scratch healed at 60 °C (b), and a scratch healed at 115 °C for a few minutes (c).

freshly made scratch (Figure 5a), the second a similar scratch that was heated to 60 °C for 2 min (Figure 5b), and the last image shows a scratch healed at 115 °C (Figure 5c). The two sides of the scratch clearly approach when heating to 60 °C. The scratch is partially healed, but at least after such a short time, some parts of the coating are still not yet fully closed. After heating to 115 °C, the sides of the scratch are again in full contact with each other, and there is almost no difference with the surrounding material.

In Figure 5a,b the area can be seen that got deformed because of scratching the coating. For the 50 μm scratch the deformed area is ~70 μm thick, which results in a compression of ~30%. (The compression gradient and three-dimensional movement of the coating are not taken into account in this simple approximation.) This is only a small deformation compared with the ones in the strain recovery experiments (see Figure 3). Therefore, better healing can be expected. Electrochemical tests presented in the next paragraph show that the healing at 60 °C for 2 min is already sufficient to regain the coatings corrosion protection and barrier properties, even if full healing is not yet achieved.

EIS gives a general picture of the corrosion protection of coatings before and after healing. Figure 6 shows the Bode plots for the amplitude of the impedance and the phase shift as a function of the frequency. Both pristine unscratched samples of the two different self-healing coatings on HDG steel described herein produce very much the same impedance spectrum (red solid line).

The red solid line in Figure 6 shows the characteristic properties of the effective barrier of the self-healing coatings, high impedance amplitudes (2×10^9 Ω cm^2 at 0.1 Hz), and almost purely capacitive behavior throughout the whole frequency

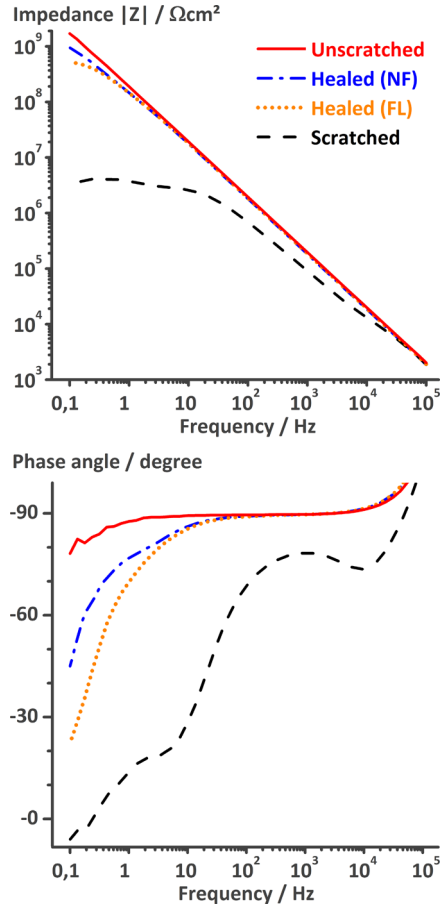

Figure 6. EIS spectra represented in Bode plots of two samples of HDG steel coated with the self-healing coating with (FL) and without (NF) flexible spacers in the polymer network before scratching, after scratching, and after heating to 60 °C for 2 min. For both networks, the spectra for the unscratched and scratched samples are the same. All measurements were recorded in 0.05 M NaCl after a stable OCP was reached within a few minutes (e.g., −0.92 V for the scratched sample).

range. The spectrum of both types of unscratched coatings remains the same, even after 13 d of neutral salt spray tests, reflecting a minimal amount of water uptake. At very high frequencies, an artifact of the measurement cell—presumably due to the reference electrode—can be seen: The phase shift lower than −90° can thus be neglected in all spectra. If a small defect similar to the ones in Figure 7a (vide infra) is made into the self-healing coating, it causes a drop of the impedance by ~2.5 decades (black dashed line). Multiplication with the estimated size of the free zinc surface results in typical impedance values for pure HDG at low frequencies (10^3–10^4 Ω cm^2 at 0.1 Hz).[43] At the same time, the phase angle increases at higher frequencies, and two new time constants appear. The process in the mid-frequency range can be assigned to the coating capacitance and pore resistance. The time constant at lower frequencies represents the ionic double layer capacitance and the polarization resistance or the corrosion reaction at the HDG surface.[44−46] The reduction of the impedance at higher frequencies shows the ingress of solution in between the coating−metal interface, as described by Gonzáles-Garcia et al.[47]

After heating the scratched sample to 60 °C for a minute, the impedance modulus returns to almost the same values as before scratching (orange dotted and blue dash-dotted line). The increase of the impedance back to ~1×10^9 Ω cm^2 (at 0.1 Hz)

DOI: 10.1021/am505621x
ACS Appl. Mater. Interfaces 2015, 7, 175−183

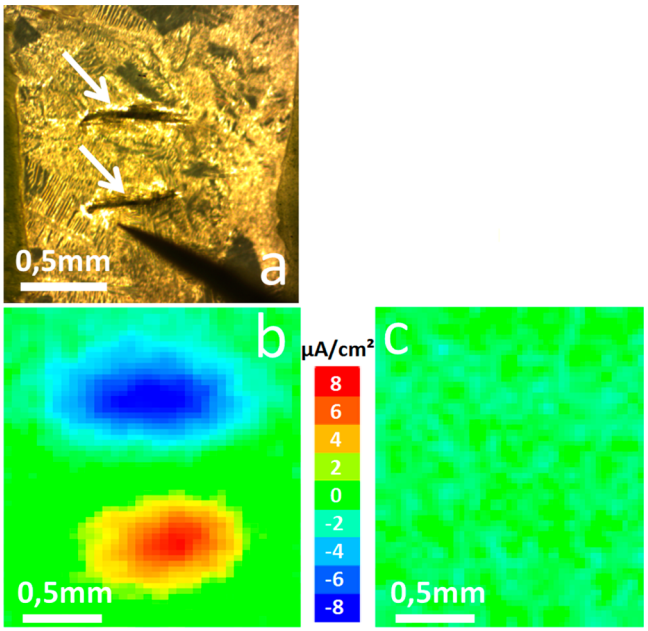

Figure 7. Optical micrograph of an HDG sample coated with the self-healing coating and two defects marked with white arrows (a). The SVET tip enters the image diagonally from the lower-right corner. Current density maps recorded with the SVET on top of the two defects before (b) and after (c) healing at 60 °C for 2 min.

and the recovery of the phase in almost the whole frequency range (until 10 Hz) prove the recovery of the barrier properties of the coatings. The small difference in the low-frequency region of the healed samples, compared with the unscratched samples, can be due to different reasons: It can be an effect of the already started corrosion process below the coating during immersion, of small pores and defects along the healed sides of the defect (Figure 5) or of a locally slightly thinner coating because of a healing efficiency below 100% (see Table 1). Generally, the performance of the two coatings is almost the same. The recovery of the self-healing coating with flexible spacers (orange dotted line, FL) is slightly below the one without flexible spacers (blue dash-dotted line, NF) when looking at their barrier properties. The results are similar to other publications used to describe coatings on metals and defects therein.[36,48−55] Trabelsi et al., for example, used electrochemical impedance spectra, together with equivalent circuit models, to explain the corrosion protection of corrosion inhibitor-doped silane coatings on galvanized steel,[55] whereas Zheludkevich et al. described the decrease of barrier properties of a hybrid sol−gel film after scratching the surface of aluminum Al2024 and the protection of the aluminum surface by 8-hydroxyquinoline using EIS.[53] Garcia-Gonzalez et al. measured the coating breakdown of a PU coating on HDG steel with EIS.[54] Their PU-coated samples immersed for a short time behave similarly to the behavior of unscratched coatings presented in this paper. When the protection of their coating is drastically reduced, the impedance Bode plots look similar to the scratched coating in Figure 6, because of the direct contact of the solution with the metallic surface. Also Jorcin et al. obtained similar results when they investigated the recovery of the barrier properties of another, thin shape memory PU coating on Al2024-T3 using ORP-EIS.[36] Because of the thickness of the self-healing coatings described in this paper, generally stronger recovery effects are observed.

Several groups showed that the combination of EIS with a local electrochemical technique like SVET has the advantage of additional certainty about the interpretation of other effects which might accidentally also be measured by EIS.[53,55−57] Figure 7b is an ionic current density map recorded in situ with SVET on top of a coated HDG steel sample with two indentations (Figure 7a) immersed in 0.05 M NaCl solution. After half an hour in solution, one distinct anodic and one distinct cathodic area are visible on the map (Figure 7b). These areas clearly have the shape and position of the two indentations made into the sample and thus can be correlated with the active corrosion of the two defects. The current densities peak at about +8 μA/cm^2 and −8 μA/cm^2 in the respective areas above the defects are several times higher than the ones measured above the intact coating and away from the defects. Next, the sample was removed from the SVET and put on a heating stage to heal the coating at 60 °C for 2 min. The healed sample produces a different current density map (Figure 7c). The current densities are clearly lower, and the anodic and cathodic areas above the healed defects are gone. Because only current fluctuations in the range of background noise can be detected, we conclude that there is no active site of corrosion present. These results confirm our interpretation of the EIS data. Figure 7b shows the two actively corroding areas of the defects that caused the drop in impedance in Figure 6 (solid red and dashed black line). The SVET map in Figure 7c proves the successful self-healing already observed by microscopy and EIS. The map is in accordance with the re-establishing of the barrier properties after healing measured by EIS.

Hereby we show that these coatings protect the metal against corrosion similar to corrosion inhibitors. Because of the short time and relatively low temperature required for healing, the necessary energy input is so low that it could even be reached by infrared lamps in a continuous production process or by washing a product with hot water. On the other hand, the coatings presented in this paper are not fully industrial products and thus currently do not contain corrosion inhibitor pigments, adhesion promoters, or leveling agents. However, they can still be embedded in these coatings to protect the metal for the period until the defects are healed. Therefore, long-term corrosion protection tests are currently ongoing to demonstrate the synergistic effects of the combination of these coatings with corrosion inhibitors.

CONCLUSION

We synthesized two shape-recovery PU−acrylate-based coatings, one with and one without flexible spacer units in the molecular network structure. High molecular weight PCL acrylates in the polymer network create the necessary mobility for self-healing of large damages upon heating above the T_m of the PCL phase. Although the two 100% UV-curable coatings show similar shape-recovery efficiencies in bulk, the coating without flexible spacers shows slightly higher toughness and mechanical strength. On the other hand, the coating with flexible spacers has a reduced onset of the healing temperature and shows better shape recovery below the T_g of the IBOA phase. The recovery of both polymer networks from 200% strain is ∼95% when slowly heated above 115 °C. Below the T_g of the IBOA phase, higher strain recovery at lower temperatures is achieved for both polymer networks if the samples are less strained. DMA experiments show the influence of the different phases of the polymer network on the self-healing ability. Additionally, repeatable shape recovery could be demonstrated by stretching followed by heating to 90 °C for 5 min and a second stretching and heating cycle. The advantage of

DOI: 10.1021/am505621x
ACS Appl. Mater. Interfaces 2015, 7, 175−183

the healing mechanism of this type of polymer network is that 96% healing efficiency (in the case of FL) can be achieved within a few minutes, compared with other mechanisms that include chemical reactions.

When applied on HDG steel, the two coatings show good mechanical properties and corrosion protection. The introduction of flexible spacers into the polymer network has no influence on these properties. Small defects in both coatings close above the melting temperature of the PCL phase, and fully disappear above the T_g of the IBOA phase. Both coatings locally lose their protection properties when scratches or indentations are applied. A short heating period of a few minutes to only 60 °C is sufficient for these coatings to heal the scratches and almost fully regain their original barrier and corrosion protection properties as shown by EIS and SVET. Interestingly, the surpassing of the melting temperature of the PCL phase seems to be sufficient for the recovery, and heating to higher temperatures is not necessary for its corrosion protection.

■ ASSOCIATED CONTENT

Supporting Information

SEC trace of R_{NF}. Video of the self-healing of three scratches in an NF sample presented in Figure 4. This material is available free of charge via the Internet at http://pubs.acs.org.

■ AUTHOR INFORMATION

Corresponding Authors

*E-mail: alexander.lutz@vub.ac.be. (A.L.)
*E-mail: Otto.vandenberg@ugent.be. (O.V.)

Author Contributions

‖These authors contributed equally.

Notes

The authors declare no competing financial interest.

■ ACKNOWLEDGMENTS

The authors wish to acknowledge Strategic Initiative Materials (SIM) and agentschap voor Innovatie door Wetenschap en Technologie (IWT) for funding the Novel Active Protection Systems on Metals (NAPROM) project as part of the SHE program on Self-Healing Engineered materials supported by SIM. The authors thank ArcelorMittal for supplying the HDG steel plates and Croda Chemicals for providing the fatty dimer diol. A.L. thanks T. Hauffman of the Research Group Electrochemical and Surface Engineering, VUB, for the useful discussions about EIS.

■ REFERENCES

(1) Landolt, D. *Corrosion and Surface Chemistry of Metals;* CRC Press: Boca Raton, FL, 2007.

(2) Kuznetsov, Y. I. *Organic Inhibitors of Corrosion of Metals;* Springer: New York, 1996.

(3) Sastri, V. S. *Corrosion Inhibitors: Principles and Applications;* Wiley: New York, 1998.

(4) Sastri, V. S. *Green Corrosion Inhibitors: Theory and Practice;* John Wiley & Sons: Hoboken, NJ, 2012.

(5) Xia, L.; Mccreery, R. L. Chemistry of a Chromate Conversion Coating on Aluminum Alloy AA2024-T3 Probed by Vibrational Spectroscopy. *J. Electrochem. Soc.* **1998**, *145* (9), 3083−3089.

(6) Kendig, M. W.; Davenport, A. J.; Isaacs, H. S. The Mechanism of Corrosion Inhibition by Chromate Conversion Coatings from X-Ray Absorption Near Edge Spectroscopy (XANES). *Corros. Sci.* **1993**, *34* (1), 41−49.

(7) Wainright, J. S.; Murphy, O. J.; Antonio, M. R. The Oxidation State and Coordination Environment of Chromium in a Sealed Anodic Aluminum Ooxide Film by X-Ray Absorption Spectroscopy. *Corros. Sci.* **1992**, *33* (2), 281−293.

(8) Zheludkevich, M. L.; Poznyak, S. K.; Rodrigues, L. M.; Raps, D.; Hack, T.; Dick, L. F.; Nunes, T.; Ferreira, M. G. S. Active Protection Coatings with Layered Double Hydroxide Nanocontainers of Corrosion Inhibitor. *Corros. Sci.* **2010**, *52* (2), 602−611.

(9) Tedim, J.; Kuznetsova, A.; Salak, A. N.; Montemor, F.; Snihirova, D.; Pilz, M.; Zheludkevich, M. L.; Ferreira, M. G. S. Zn −Al Layered Double Hydroxides as Chloride Nanotraps in Active Protective Coatings. *Corros. Sci.* **2012**, *55*, 1−4.

(10) Buchheit, R.; Guan, H.; Mahajanam, S.; Wong, F. Active Corrosion Protection and Corrosion Sensing in Chromate-Free Organic Coatings. *Prog. Org. Coat.* **2003**, *47* (3−4), 174−182.

(11) Williams, G.; Geary, S.; McMurray, H. N. Smart Release Corrosion Inhibitor Pigments Based on Organic Ion-Exchange Resins. *Corros. Sci.* **2012**, *57*, 139−147.

(12) Maia, F.; Tedim, J.; Lisenkov, A. D.; Salak, A. N.; Zheludkevich, M. L.; Maia, F.; Ferreira, G. S. Silica Nanocontainers for Active Corrosion Protection. *Nanoscale* **2012**, *4*, 1287−1298.

(13) Montemor, M. F.; Snihirova, D. V.; Taryba, M. G.; Lamaka, S. V.; Kartsonakis, I. A.; Balaskas, A. C.; Kordas, G. C.; Tedim, J.; Kuznetsova, A.; Zheludkevich, M. L.; Ferreira, M. G. S. Evaluation of Self-Healing Ability in Protective Coatings Modified with Combinations of Layered Double Hydroxides and Cerium Molibdate Nanocontainers Filled with Corrosion Inhibitors. *Electrochim. Acta* **2012**, *60*, 31−40.

(14) Li, G. L.; Schenderlein, M.; Men, Y.; Möhwald, H.; Shchukin, D. G. Monodisperse Polymeric Core-Shell Nanocontainers for Organic Self-Healing Anticorrosion Coatings. *Adv. Mater. Interfaces*, **2014**. DOI 10.1002/admi.201300019.

(15) Guan, H.; Buchheit, R. G. Corrosion Protection of Aluminum Alloy 2024-T3 by Vanadate Conversion Coatings. *Corrosion* **2004**, *60* (3), 284−296.

(16) Williams, G.; McMurray, H. N. Inhibition of Filiform Corrosion on Organic-Coated AA2024-T3 by Smart-Release Cation and Anion-Exchange Pigments. *Electrochim. Acta* **2012**, *69*, 287−294.

(17) Kartsonakis, I. a.; Athanasopoulou, E.; Snihirova, D.; Martins, B.; Koklioti, M. a.; Montemor, M. F.; Kordas, G.; Charitidis, C. a. Multifunctional Epoxy Coatings Combining a Mixture of Traps and Inhibitor Loaded Nanocontainers for Corrosion Protection of AA2024-T3. *Corros. Sci.* **2014**, *85*, 147−159.

(18) Blaiszik, B. J.; Sottos, N. R.; White, S. R. Nanocapsules for Self-Healing Materials. *Compos. Sci. Technol.* **2008**, *68* (3−4), 978−986.

(19) Caruso, M. M.; Delafuente, D. a.; Ho, V.; Sottos, N. R.; Moore, J. S.; White, S. R. Solvent-Promoted Self-Healing Epoxy Materials. *Macromolecules* **2007**, *40* (25), 8830−8832.

(20) Zadeh, M. A.; Garcia, S. J.; van der Zwaag, S. Routes to Extrinsic and Intrinsic Self-Healing Corrosion Protective Sol-Gel Coatings: A Review. *Self-Healing Mater.* **2013**, *1*, 1−18.

(21) Toohey, K. S.; Sottos, N. R.; Lewis, J. a; Moore, J. S.; White, S. R. Self-Healing Materials with Microvascular Networks. *Nat. Mater.* **2007**, *6* (8), 581−585.

(22) Norris, C. J.; Meadway, G. J.; O'Sullivan, M. J.; Bond, I. P.; Trask, R. S. Self-Healing Fibre Reinforced Composites via a Bioinspired Vasculature. *Adv. Funct. Mater.* **2011**, *21* (19), 3624−3633.

(23) Hansen, C. J.; Wu, W.; Toohey, K. S.; Sottos, N. R.; White, S. R.; Lewis, J. a. Self-Healing Materials with Interpenetrating Microvascular Networks. *Adv. Mater.* **2009**, *21* (41), 4143−4147.

(24) Billiet, S.; Hillewaere, X. K. D.; Teixeira, R. F. a; Du Prez, F. E. Chemistry of Crosslinking Processes for Self-Healing Polymers. *Macromol. Rapid Commun.* **2013**, *34* (4), 290−309.

(25) García, S. J.; Fischer, H. R.; van der Zwaag, S. A Critical Appraisal of the Potential of Self Healing Polymeric Coatings. *Prog. Org. Coat.* **2011**, *72* (3), 211−221.

(26) González-García, Y.; Mol, J. M. C.; Muselle, T.; De Graeve, I.; Van Assche, G.; Scheltjens, G.; Van Mele, B.; Terryn, H. SECM Study of Defect Repair in Self-Healing Polymer Coatings on Metals. *Electrochem. Commun.* **2011**, *13* (2), 169−173.

DOI: 10.1021/am505621x
ACS Appl. Mater. Interfaces 2015, 7, 175−183

(27) Scheltjens, G.; Diaz, M. M.; Brancart, J.; Van Assche, G.; Van Mele, B. A Self-Healing Polymer Network Based on Reversible Covalent Bonding. *React. Funct. Polym.* **2013**, *73* (2), 413−420.
(28) Wouters, M.; Craenmehr, E.; Tempelaars, K.; Fischer, H.; Stroeks, N.; van Zanten, J. Preparation and Properties of a Novel Remendable Coating Concept. *Prog. Org. Coat.* **2009**, *64* (2−3), 156−162.
(29) Tian, Q.; Rong, M. Z.; Zhang, M. Q.; Yuan, Y. C. Synthesis and Characterization of Epoxy with Improved Thermal Remendability Based on Diels-Alder Reaction. *Polym. Int.* **2010**, *59* (10), 1339−1345.
(30) Scheltjens, G.; Brancart, J.; Graeve, I.; Mele, B.; Terryn, H.; Assche, G. Self-Healing Property Characterization of Reversible Thermoset Coatings. *J. Therm. Anal. Calorim.* **2011**, *105* (3), 805−809.
(31) Canadell, J.; Goossens, H.; Klumperman, B. Self-Healing Materials Based on Disulfide Links. *Macromolecules* **2011**, *44* (8), 2536−2541.
(32) Jones, A. R.; Cintora, A.; White, S. R.; Sottos, N. R. Autonomic Healing of Carbon Fiber/Epoxy Interfaces. *ACS Appl. Mater. Interfaces* **2014**, *6* (9), 6033−6039.
(33) Rodriguez, E. D.; Luo, X.; Mather, P. T. Linear/Network Poly(ε-caprolactone) Blends Exhibiting Shape Memory Assisted Self-Healing (SMASH). *ACS Appl. Mater. Interfaces* **2011**, *3* (2), 152−161.
(34) Rivero, G.; Nguyen, L.-T. T.; Hillewaere, X. K. D.; Du Prez, F. E. One-Pot Thermo-Remendable Shape Memory Polyurethanes. *Macromolecules* **2014**, *47* (6), 2010−2018.
(35) D'Hollander, S.; Van Assche, G.; Van Mele, B.; Du Prez, F. Novel Synthetic Strategy Toward Shape Memory Polyurethanes with a Well-Defined Switching Temperature. *Polymer.* **2009**, *50* (19), 4447−4454.
(36) Jorcin, J.-B.; Scheltjens, G.; Van Ingelgem, Y.; Tourwé, E.; Van Assche, G.; De Graeve, I.; Van Mele, B.; Terryn, H.; Hubin, A. Investigation of the Self-Healing Properties of Shape Memory Polyurethane Coatings with the "Odd Random Phase Multisine" Electrochemical Impedance Spectroscopy. *Electrochim. Acta* **2010**, *55* (21), 6195−6203.
(37) Smith, O. W.; Weigel, J. E.; Trecker, D. J. United States Patent Reissue 29,131, 1977.
(38) Nabeth, B.; Gerard, J. F.; Pascault, J. P. Dynamic Mechanical Properties of UV Curable Polyurethane Acrylate with Various Reactive Diluents. *J. Appl. Polym. Sci.* **1996**, *60* (12), 2113−2123.
(39) Esteves, A. C. C.; Lyakhova, K.; van Riel, J. M.; van der Ven, L. G. J.; van Benthem, R. a T. M.; de With, G. Self-Replenishing Ability of Cross-Linked Low Surface Energy Polymer Films Investigated by a Complementary Experimental-Simulation Approach. *J. Chem. Phys.* **2014**, *140* (12), 124902.
(40) Ghodsieh, M.; Ebrahimi, M.; Bastani, S. UV Curable Urethane Acrylate Coatings Formulation: Experimental Design Approach. *Pigm. Resin Technol.* **1972**, *43* (2), 61−68.
(41) Koleske, J. V. *Paint and Coating Testing Manual (Gardner-Sward Handbook),* 15th ed.; ASTM International: West Conshohocken, PA, 1995.
(42) Brandrup, J.; Immergut, E. H.; Grulke, E. A. *Polymer Handbook,* 4th ed; Wiley-Interscience: New York, 1999.
(43) Jorcin, J.-B.; Aragon, E.; Merlatti, C.; Pébère, N. Delaminated Areas Beneath Organic Coating: A Local Electrochemical Impedance Approach. *Corros. Sci.* **2006**, *48* (7), 1779−1790.
(44) Bastos, a. C.; Ferreira, M. G. S.; Simões, A. M. Comparative Electrochemical Studies of Zinc Chromate and Zinc Phosphate as Corrosion Inhibitors for Zinc. *Prog. Org. Coat.* **2005**, *52* (4), 339−350.
(45) Jorcin, J.-B.; Orazem, M. E.; Pébère, N.; Tribollet, B. CPE Analysis by Local Electrochemical Impedance Spectroscopy. *Electrochim. Acta* **2006**, *51* (8−9), 1473−1479.
(46) Trabelsi, W.; Triki, E.; Dhouibi, L.; Ferreira, M. G. S.; Zheludkevich, M. L.; Montemor, M. F. The Use of Pre-Treatments Based on Doped Silane Solutions for Improved Corrosion Resistance of Galvanised Steel Substrates. *Surf. Coat. Technol.* **2006**, *200* (14−15), 4240−4250.
(47) González-García, Y.; González, S.; Souto, R. M. Electrochemical and Structural Properties of a Polyurethane Coating on Steel Substrates for Corrosion Protection. *Corros. Sci.* **2007**, *49* (9), 3514−3526.
(48) Beaunier, L.; Epelboin, I.; Lestrade, J. C.; Takenouti, H. Etude Electrochimique, et par Microscopie Electronique a Balayage, du Fer Recouvert de Peinture. *Surf. Technol.* **1976**, *4* (3), 237−254.
(49) Bastos, a. C.; Ostwald, C.; Engl, L.; Grundmeier, G.; Simões, A. M. Formability of Organic Coatings-an Electrochemical Approach. *Electrochim. Acta* **2004**, *49* (22−23), 3947−3955.
(50) Mansfeld, F.; Han, L. T.; Lee, C. C.; Zhang, G. Evaluation of Corrosion Protection by Polymer Coatings Using Electrochemical Impedance Spectroscopy and Noise Analysis. *Electrochim. Acta* **1998**, *43* (19−20), 2933−2945.
(51) Deflorian, F.; Fedrizzi, L.; Bonora, P. L. Determination of the Reactive Area of Organic Coated Metals: Physical Meaning and Limits of the Break-Point Method. *Electrochim. Acta* **1993**, *38* (12), 1609−1613.
(52) Bonora, P. L.; Deflorian, F.; Fedrizzi, L. Electrochemical Impedance Spectroscopy as a Tool for Investigating Underpaint Corrosion. *Electrochim. Acta* **1996**, *41* (7−8), 1073−1082.
(53) Zheludkevich, M. L.; Yasakau, K. A.; Bastos, A. C.; Karavai, O. V.; Ferreira, M. G. S. On the Application of Electrochemical Impedance Spectroscopy to Study the Self-Healing Properties of Protective Coatings. *Electrochem. Commun.* **2007**, *9*, 2622−2628.
(54) González-García, Y.; Gonzalez, S.; Souto, R. Electrochemical and Structural Properties of a Polyurethane Coating on Steel Substrates for Corrosion Protection. *Corros. Sci.* **2007**, *49* (9), 3514−3526.
(55) Trabelsi, W.; Cecilio, P.; Ferreira, M.; Montemor, M. Electrochemical Assessment of the Self-Healing Properties of Ce-Doped Silane Solutions for the Pre-Treatment of Galvanised Steel Substrates. *Prog. Org. Coat.* **2005**, *54* (4), 276−284.
(56) Khramov, A. N.; Balbyshev, V. N.; Voevodin, N. N.; Donley, M. S. Nanostructured Sol−Gel Derived Conversion Coatings Based on Epoxy- and Amino-silanes. *Prog. Org. Coat.* **2003**, *47* (3−4), 207−213.
(57) Grundmeier, G.; Schmidt, W.; Stratmann, M. Corrosion Protection by Organic Coatings: Electrochemical Mechanism and Novel Methods of Investigation. *Electrochim. Acta* **2000**, *45* (15−16), 2515−2533.

NOTE ADDED AFTER ASAP PUBLICATION

This paper posted ASAP on December 30, 2014. Figure 6 was replaced and text relating to it was corrected. The revised version was reposted on January 14, 2015.

DOI: 10.1021/am505621x
ACS Appl. Mater. Interfaces 2015, 7, 175−183